

Non-Faradaic Electrochemical Modification of Catalytic Activity

9. Ethylene Oxidation on Pt Deposited on TiO₂

C. Pliangos, I. V. Yentekakis, S. Ladas, and C. G. Vayenas

Department of Chemical Engineering, University of Patras, Patras GR-26500, Greece

Received April 3, 1995; revised November 20, 1995; accepted November 27, 1995

The catalytic activity of Pt for the oxidation of ethylene to CO₂ can be markedly and reversibly affected by interfacing polycrystalline Pt films with TiO₂ and applying currents or potentials between the catalyst film and a Au counter electrode at temperatures near 500°C. The increase in the rate of C₂H₄ oxidation is up to 20 times higher than the open-circuit (unpromoted) catalytic rate and at least a factor of 5000 higher than the rate of O²⁻ supply through the mixed conducting TiO₂ support. The latter is and remains catalytically inert during electrical bias. This electrochemically induced Schwab effect of the second kind has all the same qualitative features with the effect of non-Faradaic electrochemical modification of catalytic activity (NEMCA effect) when using pure O²⁻ conductors. Work function measurements and X-ray photoelectron spectroscopic (XPS) investigation of the Pt catalyst surface under UHV conditions has also provided evidence consistent with the electrochemically controlled promoting oxide ion backspillover mechanism which is operative with NEMCA when using pure O²⁻ conductors. Under reaction conditions in atmospheric pressure or oxidizing environments in UHV the TiO₂ support exhibits mixed electronic (*n*-type)-ionic conductivity and thus the catalyst work function and catalytic activity can be controlled by the applied potential. In reducing environments the electronic conductivity of TiO₂ dominates and the catalyst work function remains constant upon application of potential. © 1996 Academic Press, Inc.

INTRODUCTION

The effect of non-Faradaic electrochemical modification of catalytic activity (NEMCA effect) has been described for over thirty catalytic reactions on Pt, Pd, Rh, Ag, Ni, and IrO₂ catalysts deposited on O²⁻, Na⁺, F⁻, and H⁺ solid state ionic conductors (1–14). More recently the effect has also been demonstrated using aqueous alkaline solutions (15). In brief, it has been found that the catalytic activity and selectivity of metal films interfaced with solid electrolyte components can be markedly and reversibly controlled by applying currents or potentials (± 2 V) between the catalyst film and a counter electrode deposited on the same solid electrolyte component, thus forming the galvanic cell:

Gaseous reactants, (e.g., C ₂ H ₄ + O ₂),	Solid electrolyte (e.g., 8 mol% Y ₂ O ₃ -stabilized ZrO ₂)	Counter electrode, (e.g., Ag),
metal catalyst (e.g., Pt)		Auxiliary gas (e.g., O ₂)

The increase in the catalytic rate on the metal catalyst is up to 100 times larger than the open-circuit (unpromoted) rate and up to 3×10^5 times higher than the rate $I/2F$ of supply of ions to the catalyst surface. It has been shown by several techniques, including X-ray photoelectron spectroscopy (XPS) (16), surface enhanced Raman spectroscopy (SERS) (17), temperature-programmed desorption (TPD) (18), and work function measurements (3), that the NEMCA effect is due to an electrochemically controlled backspillover (migration) of ions from the solid electrolyte onto the catalyst surface. These chemisorbed backspillover species act as promoters for catalytic reactions by affecting the binding strength of chemisorbed reactants and reaction intermediates (7, 20). Consequently the NEMCA effect is the result of a controlled *in situ* introduction of dopants on catalyst surfaces and therefore the terms “*in situ* controlled promotion” (10) or “electrochemical promotion” (4) have been also used to describe NEMCA, which does not appear to be limited to any particular group of catalytic reactions, metals, or solid electrolytes (1–21). Work in this area has been recently reviewed (7, 19–21) and the importance of NEMCA in catalysis and electrochemistry has been discussed by Pritchard (4) and Bockris (22), respectively.

Previous NEMCA studies have utilized pure ionic conductors as the solid electrolyte, i.e., 8 mol% Y₂O₃-stabilized-ZrO₂ (1–3, 8, 9, 13, 14), an O²⁻ conductor, β'' -Al₂O₃ (6, 10–12), a Na⁺ conductor, CaF₂ (20), a F⁻ conductor and H⁺ conductors such as C₆H₅SO₄ (5) and Nafion (20, and references therein). These solid electrolytes, which under electrical bias (NEMCA) conditions behave as reversible doping ion donors, have a negligible electronic conductivity.

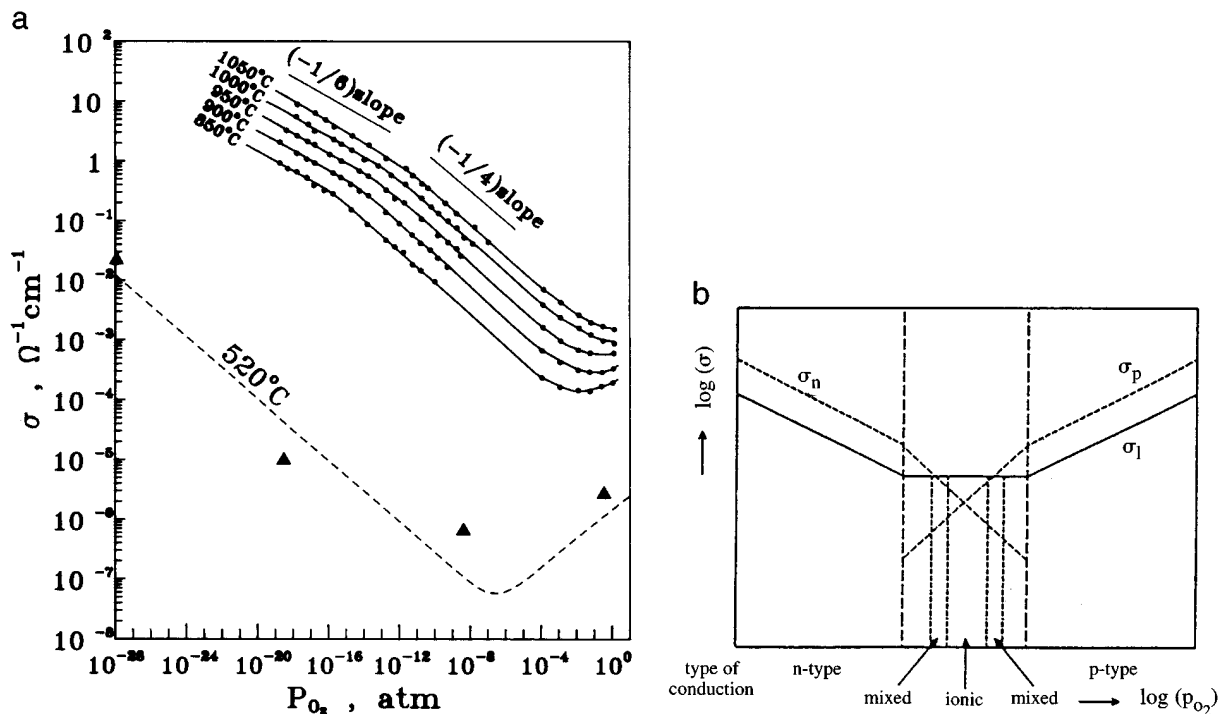


FIG. 1. (a) Effect of oxygen activity and temperature on the electrical conductivity of TiO_2 (\bullet , Ref. (36), \blacktriangle , present work). (b) Idealized Brouwer plot of an MO_2 oxide, showing the effect of oxygen activity on the electrical conductivity of mixed-conducting oxides and the relative contribution of n - and p -type semiconductivity and of ionic conductivity.

In the present study TiO_2 was used instead of a solid electrolyte in the cell



and the effect was examined of applying constant currents or potentials on the rate of the oxidation of ethylene on the Pt catalyst. As in NEMCA studies, dramatic and reversible alterations in catalytic rate were observed.

Titania is an important support material from a practical point of view but most importantly from a fundamental point of view. It has been studied extensively in the context of metal-support interactions and in particular that of strong metal-support interactions (SMSI) (23–27). The relevant literature has been reviewed by Tauster (28) and by Haller and Resasco (29). The origin of the classical SMSI effect has been shown to be metal decoration by TiO_x moieties (24–27).

In addition to its importance as a metal support material, TiO_2 is a very significant material in sensor technology (30) due to its predominantly n -type semiconductivity and concomitant marked variation in electronic conductivity with oxygen chemical potential (30, 31). The Pt/ TiO_2 interface, in particular, has been studied in detail for sensor application using a variety of surface spectroscopic techniques (32–34). Depending on the temperature of preparation and gaseous composition this interface can exhibit Schottky-type or ohmic behavior (33).

One important material property of TiO_2 , which has not attracted attention in the catalytic literature, is that TiO_2 is a mixed conductor, i.e., in addition to n -type semiconductivity at low P_{O_2} values and p -type semiconductivity at high P_{O_2} values, it also exhibits some ionic conductivity due to migration of O^{2-} ions or vacancies (35, 36) and/or protons (37, 38). As shown in Fig. 1, the relative importance of the ionic conductivity can be significant at intermediate or high P_{O_2} values, while at low P_{O_2} n -type semiconductivity totally dominates (36).

No attempt will be made here to address the possible relevance of this important and neglected material property of TiO_2 (Fig. 1) with the SMSI effect, but it will become apparent below that Fig. 1 is essential in understanding the observed pronounced non-Faradaic catalytic rate enhancement obtained in this work for Pt films interfaced with TiO_2 .

EXPERIMENTAL

The apparatus used for atmospheric pressure kinetic studies utilizing on-line gas chromatography (Perkin-Elmer 300B), mass spectrometry (Balzers QMG 311), and IR spectroscopy (Beckman 864 CO_2 analyzer) has been described previously (2, 6, 7).

Reactants were Messer Griesheim certified standards of C_2H_4 in He and O_2 in He. They could be further diluted in ultrapure (99.999%) He (L'Air Liquide).

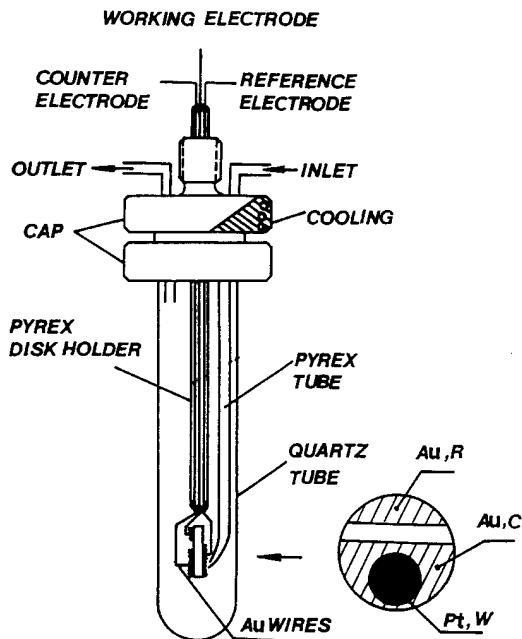


FIG. 2. Single-pellet reactor. The auxiliary Au electrodes are deposited on one side of the TiO₂ disc and the Pt catalyst on the other.

The atmospheric pressure quartz reactor shown schematically in Fig. 2 has been described previously (7, 10). It has a volume of 30 cm³ and behaves as a CSTR in the flowrate range of 50–300 cm³ STP/min, as shown previously by determination of its residence time distribution using the IR CO₂ analyzer (7). The conversion of the reactants under open- and closed-circuit conditions was kept below 20%.

The TiO₂ tablet (Merck Titanium (IV) Oxide Patinal, 11495) was suspended in the quartz reactor by means of the Au wires attached to the three electrodes. The electrode arrangement is shown in Fig. 2. Prior to catalyst deposition, the TiO₂ tablet was sintered for 2 h at 1000°C. This should suffice for almost complete conversion of any anatase to rutile.

The Pt catalyst electrode was deposited on one side of the TiO₂ tablet by application of a thin coating of Engelhard Pt paste A-1121 followed by drying and calcination first (3°C/min) to 450°C for 1 h and then (2°C/min) to 830°C for 1 h. The Pt catalyst surface area (reactive oxygen uptake) was measured via surface titration of oxygen with C₂H₄ at 500°C and found to be 1.9×10^{-7} mol O. Typical scanning electron micrographs of the Pt catalyst film are shown in Fig. 3.

Gold counter and reference electrodes were deposited on the opposite side of the TiO₂ tablet by using a Au paste prepared by mixing Au powder (Aldrich powder 99.9+, 32,658-5) in a slurry of poly-vinyl acetate binder in ethyl acetate and following the same calcination procedure as with the Pt catalyst.

A series of blank experiments showed that the TiO₂ tablet and the Au electrodes were inactive for C₂H₄ oxidation at temperatures up to 540°C.

In the same series of blank experiments (no Pt catalyst-electrode) currents up to 100 μA were applied between the two Au electrodes without any induction of catalytic activity for C₂H₄ oxidation. Consequently all the observed catalytic phenomena can be safely attributed to the Pt catalyst only.

The experimental setup used to carry out the XPS investigation has been described previously (16). A 2-mm-thick TiO₂ slab (10 mm × 13 mm) with a Pt catalyst film, Pt reference electrode (deposited on the same side of the TiO₂ slab), and Ag counter electrode was mounted on a resistively heated Mo holder in an ultrahigh vacuum (UHV) chamber (base pressure 7×10^{-8} Pa) and the catalyst film (9 mm × 9 mm) was examined at temperatures 25 to 520°C by X-ray photoelectron spectroscopy (XPS) using a Leybold HS-12 analyzer operated at constant ΔE mode with 100-eV pass energy and a sampling area of 5 mm × 3 mm. Materials (TiO₂, Pt) and Pt catalyst deposition procedure were identical with the samples used for the atmospheric pressure kinetic study. Electron binding energies have been referenced to the metallic Pt 4f_{7/2} peak of the grounded catalyst at 71.1 eV, which always remains unchanged with no trace of nonmetallic (i.e., PtO₂) components. Since the Pt catalyst film is porous the XPS signal contains a contribution from the TiO₂ surface as well, which is visible through the microcracks of the Pt film (Fig. 3). In order to verify that the Ti XPS signal originated from the TiO₂ surface and not from TiO_x which might have migrated on the Pt electrode surface during catalyst preparation the catalyst surface was ion sputtered (Ar⁺) for 30 min without any loss in the intensity of the Ti XPS signal. As shown in the results section, this Ti XPS signal is very useful for studying the Pt–TiO₂ interface.

Changes $\Delta(e\Phi)$ in the work function $e\Phi$ of the Pt catalyst film were monitored by a Kelvin probe (Besocke/Delta-Phi-Electronik, probe "S") with a 2.5 mm diameter Au-grid vibrating condenser element placed ~ 500 μm from the Pt surface in the UHV system. As previously discussed (3, 39), in the Kelvin probe "S" operation the CPD signal is drawn from the vibrating Au grid so that the Kelvin probe lock-in amplifier circuit is entirely independent of the electrochemical circuit of the TiO₂ sample.

RESULTS

Current–Potential Behavior

Figures 4 and 5 show typical current–potential curves in terms of the catalyst potential (working electrode, W) with respect to the reference electrode (R), denoted by V_{WR} . These plots were obtained both under atmospheric pressure conditions (Fig. 4) with various gaseous environments ranging from 2 kPa H₂ to 20 kPa O₂ and also under vacuum

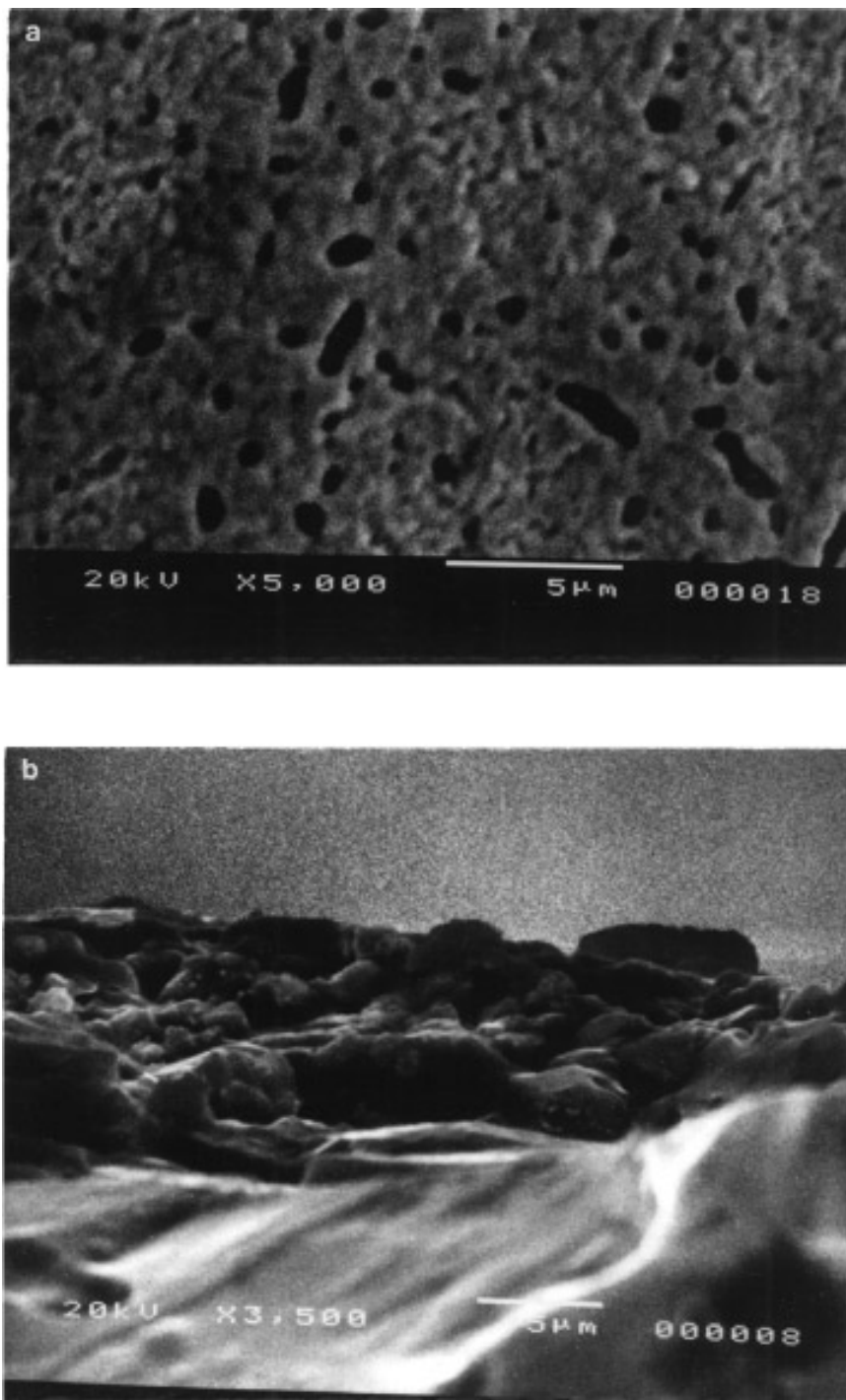


FIG. 3. Scanning electron micrographs of the Pt catalyst film: (a) top view, (b) cross section showing the Pt-TiO₂ interface.

conditions (Fig. 5) with $P_{\text{H}_2} = 30$ mPa or $P_{\text{O}_2} = 45$ mPa.

In both cases the plots are linear for reducing gaseous environments. Under these conditions the current-potential behavior is dominated entirely by the ohmic resistance of the TiO₂ sample. There is a dramatic increase of 4 orders of magnitude in the sample resistivity as one goes from

$P_{\text{H}_2} = 2$ kPa to $P_{\text{O}_2} = 20$ kPa and this is consistent with the *n*-type semiconductivity of TiO₂ (Fig. 1). For oxidizing conditions and also for mixed reactant (C₂H₄ + O₂) feeds deviations from linearity appear which are almost symmetric for positive and negative currents and thus provide no sign of Schottky-type behavior at the Pt-TiO₂ interface. In the

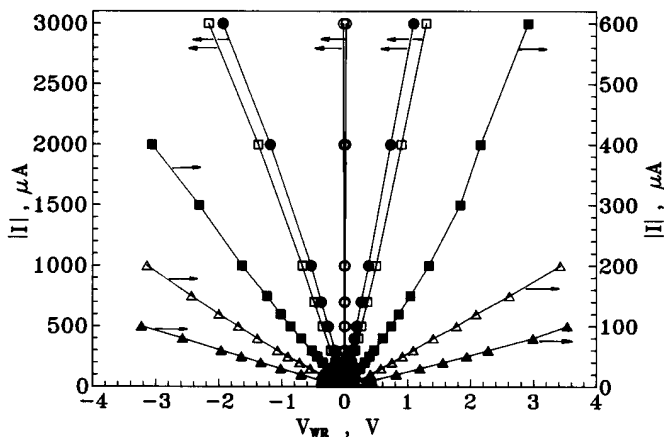


FIG. 4. Effect of current on catalyst potential at atmospheric pressure: (Δ) $P_{O_2} = 20$ kPa, (Δ) $P_{O_2} = 9.7$ kPa, $P_{C_2H_4} = 1$ kPa; (\blacksquare) $P_{O_2} = 1$ kPa, $P_{C_2H_4} = 1.2$ kPa, (\square) $P_{O_2} = 1$ kPa, $P_{C_2H_4} = 10$ kPa; (\bullet) $P_{C_2H_4} = 11$ kPa, (\circ) $P_{H_2} = 2$ kPa.

case of Schottky-type interfaces the current-potential plots are strongly asymmetric with respect to zero applied potential with the current increasing exponentially with potential upon forward bias and practically vanishing upon reverse bias (30, 32–34).

This symmetry is also shown in Fig. 6, which presents results obtained under reaction conditions in the log I vs V_{WR} (Tafel) mode, as in previous NEMCA studies (7, 20, 21). The extracted anodic and cathodic transfer coefficients α_a and α_c obtained by fitting these data to the Butler-Volmer equation

$$\ln(I/I_0) = \alpha_a F \Delta V_{WR} / RT - \alpha_c F \Delta V_{WR} / RT \quad [1]$$

are too small, of the order of 0.05 each, indicating again

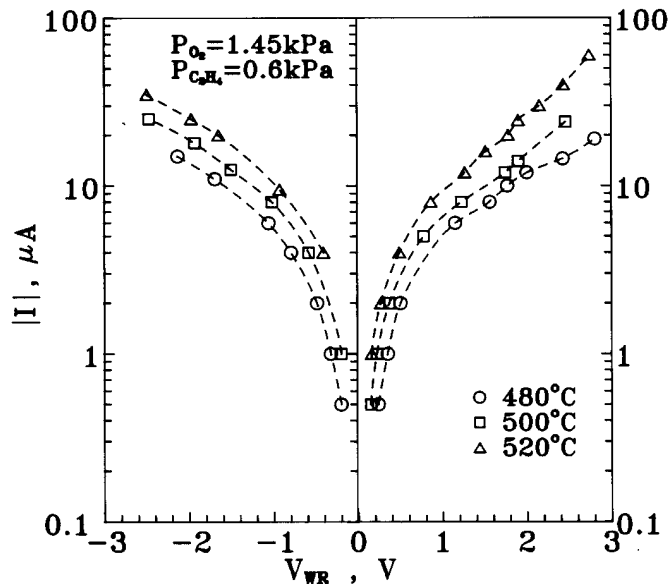
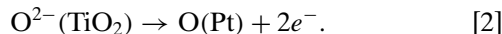


FIG. 6. Current-potential plots under reaction conditions.

the very pronounced contribution of the electronic current between TiO₂ and Pt vs charge transfer (ionic) current from



Nevertheless the onset of the above charge transfer contribution, i.e., the creation of an electrochemical double layer (20) at the Pt-TiO₂ interface under oxidizing and catalytic reaction conditions is also manifested by the slow approach to steady state of the catalyst potential during galvanostatic transients under these conditions (Fig. 7) and more clearly by the work function and XPS measurements as analyzed below.

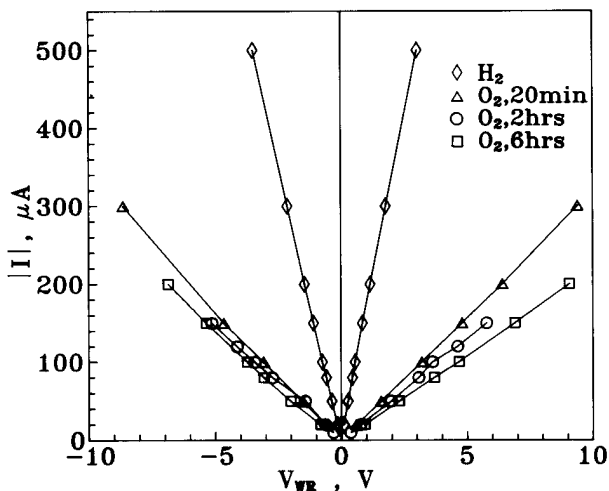


FIG. 5. Effect of current on catalyst potential under vacuum conditions; $P_{H_2} = 30$ mPa, $P_{O_2} = 45$ mPa.

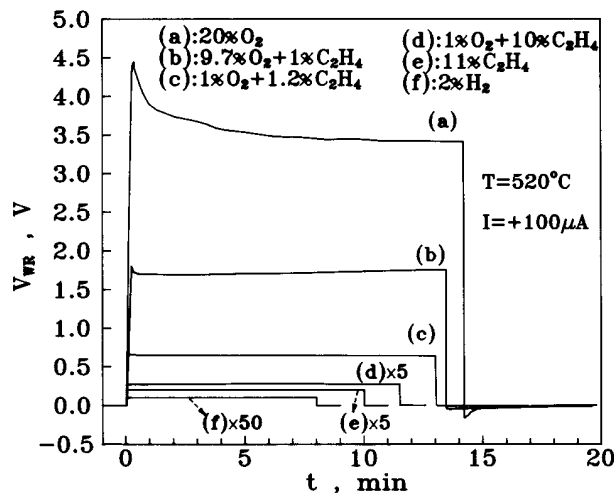


FIG. 7. Transient effect of applied current ($100 \mu\text{A}$) on catalyst potential at various atmospheric pressure compositions.

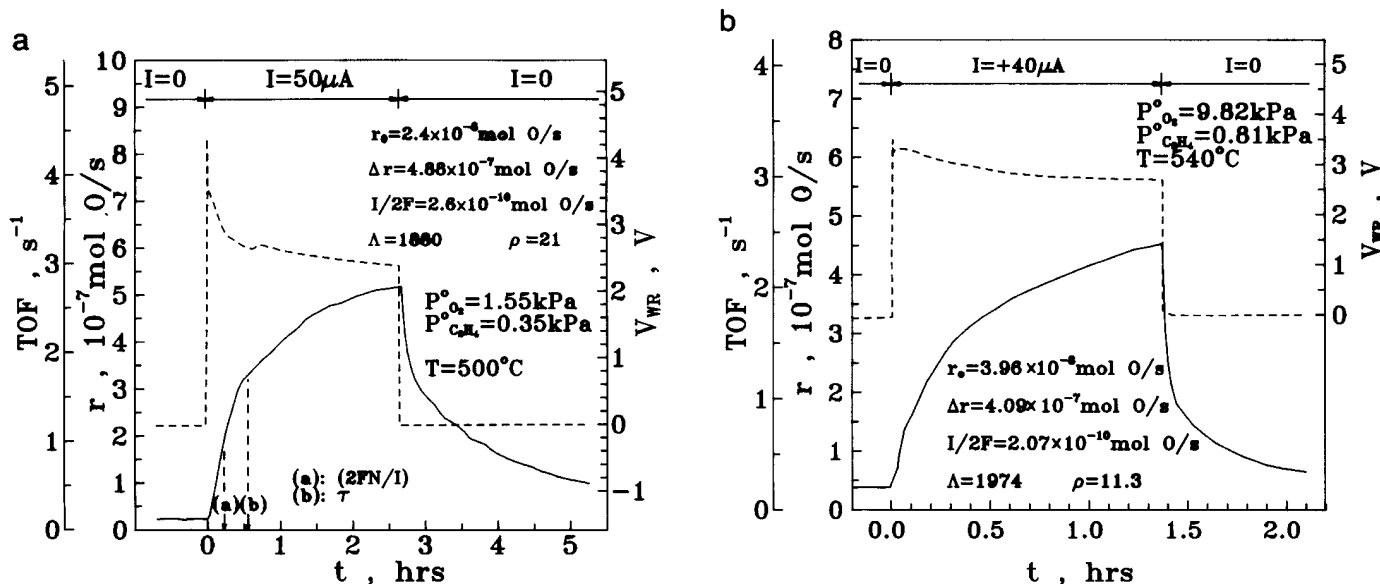


FIG. 8. Transient effect of applied positive current on the rate and turnover frequency of C_2H_4 oxidation on Pt/TiO₂ (solid curve) and on catalyst potential (dashed curve) at high (a) and very high (b) oxygen to ethylene ratios.

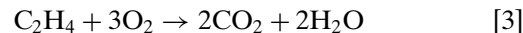
NEMCA: Catalytic Rate Transients upon Imposition of Constant Current

Figures 8 and 9 show typical galvanostatic rate transients, i.e., they depict the effect of constant applied current between the Pt catalyst and the Au counter electrode on the rate of C_2H_4 oxidation on the Pt catalyst. Figures 8 and 9 correspond to the application of positive current (i.e., the catalyst is made positive relative to the counter electrode) and negative current respectively.

As shown in Figures 8 and 9 and further analyzed below, positive currents (i.e., increasing catalyst potential V_{WR})

always causes an increase in the catalytic rate whereas negative current application leads to a rate decrease under oxidizing conditions and to a rate increase under reducing conditions.

Referring to Fig. 8a, the steady state open-circuit ($I=0$) catalytic rate of C_2H_4 oxidation



is 2.4×10^{-8} mol O/s and the corresponding turnover frequency (TOF), i.e., oxygen atoms reacting per surface Pt site per s is 0.12.

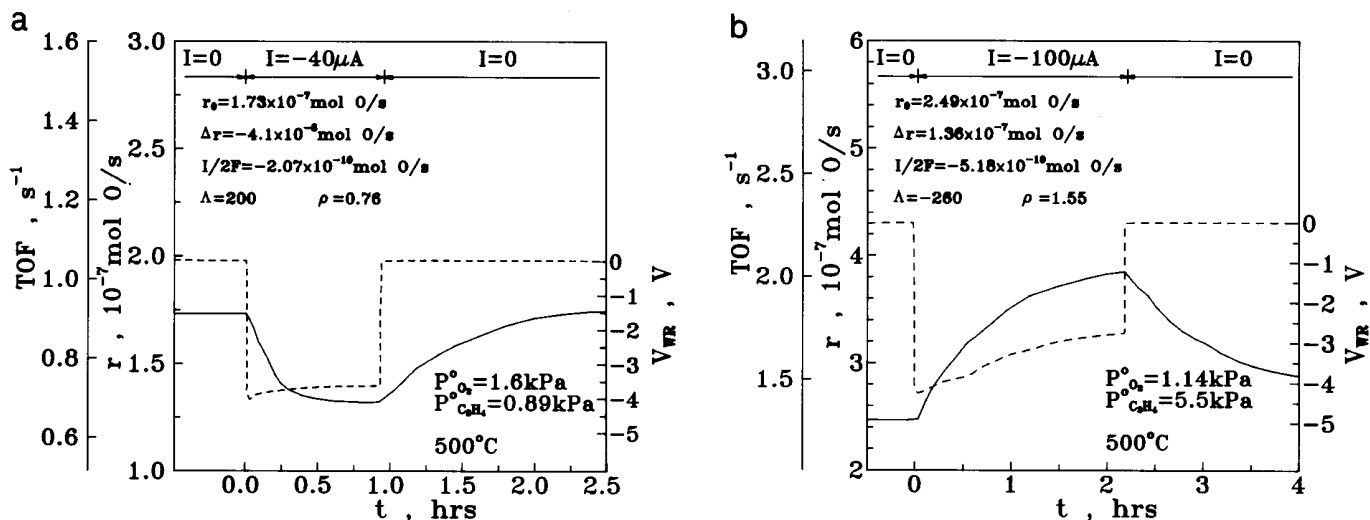


FIG. 9. Transient effect of applied negative current on the rate and turnover frequency of C_2H_4 oxidation on Pt/TiO₂ (solid curve) and on catalyst potential (dashed curve) at high (a) and low (b) oxygen to ethylene ratios.

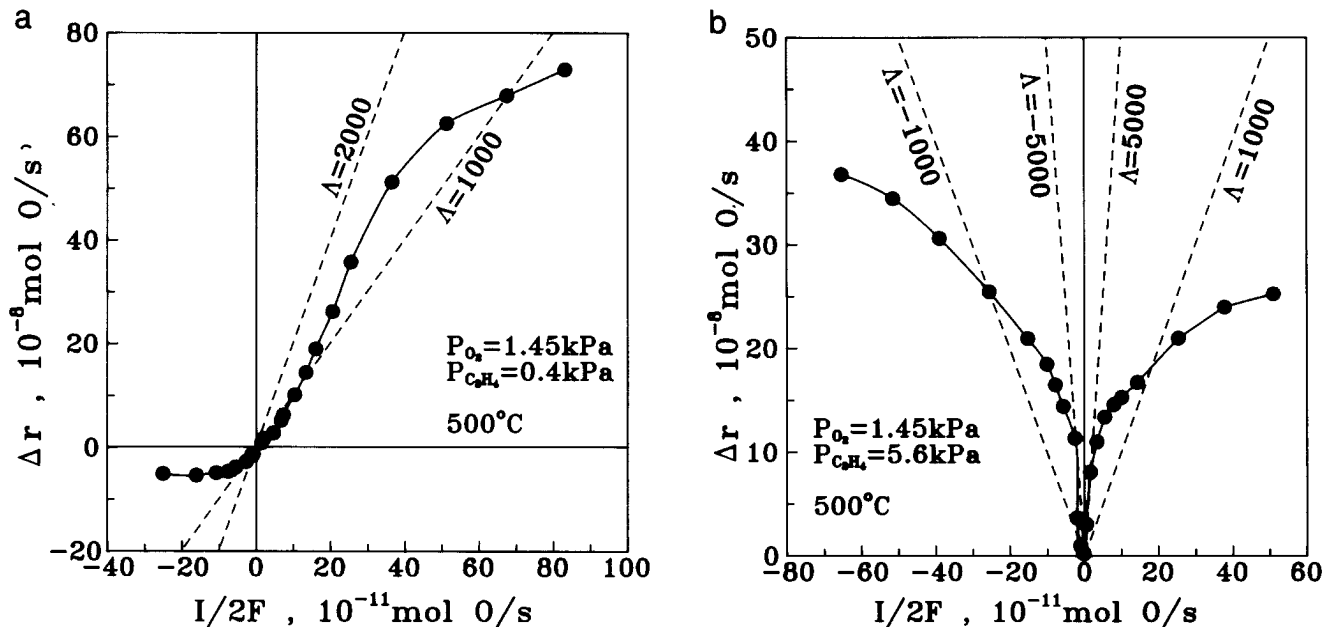


FIG. 10. Effect of applied current on the change in the rate of C₂H₄ oxidation on Pt/TiO₂ for high (a) and low (b) oxygen to ethylene ratios. Dashed lines are constant enhancement factor (Faradaic efficiency) lines.

Application of a positive current $I = 50 \mu\text{A}$ causes a reversible 20-fold increase in the catalytic rate over a period of approximately 3 h, i.e., the reaction exhibits electrophobic behavior as in previous studies of C₂H₄ oxidation on Pt deposited on YSZ (2, 7) or β'' -Al₂O₃ (6, 7). Upon current interruption the catalytic rate returns to its initial value over a period of 3–4 h. The rate increase $\Delta r = 4.88 \times 10^{-7} \text{ mol O/s}$ is 20 times larger than the open-circuit (unpromoted) rate and 1880 times larger than $I/2F$, which expresses the rate of O²⁻ transport to the Pt catalyst from the TiO₂ support, if all the current is ionic. Consequently the rate enhancement ratio ρ and the enhancement factor Λ defined from (1–15),

$$\rho = r/r_0; \quad \Lambda = \Delta r/(I/2F), \quad [4]$$

are 21 and 1880, respectively, for the experiment in Fig. 8a.

As previously noted only a small fraction f of the applied current is ionic and the remaining fraction $(1-f)$ is electronic. This means that the rate of O²⁻ supply to the catalyst is only $f(I/2F)$ and thus the promoting action of the oxide ions is even more pronounced than the measured Λ value implies.

As also shown in Fig. 8a the catalytic rate relaxation time constant τ (defined as the time required for the rate increase to reach 63% of its steady-state value) is a factor of 3 larger than $2FN/I$ (N is the Pt catalyst surface area in mol O), which expresses the time required to form a monolayer of backspillover oxidic oxygen on the Pt surface if all the current is ionic. Previous NEMCA studies with ZrO₂ (8 mol% Y₂O₃) have shown that τ is of the same order of magnitude but is typically a factor of 2 shorter than $2FN/I$.

The fact that here the opposite trend is observed is consistent with the fact that only fraction f (~ 0.1 – 0.2 at most as shown later) of the current is ionic.

Figure 8b shows a similar transient under strongly oxidizing conditions. The corresponding ρ and Λ values are here 11.3 and 1970, respectively.

It is worth noting the peculiar V_{WR} transient behavior in Figs. 8 and 9. This type of behavior indicates a gradual asymptotic decrease in the charge-transfer resistance with constant applied current and may result from the gradual change in the coverage of chemisorbed oxygen and ethylene in the vicinity of the three-phase boundaries (tpb) Pt–TiO₂–gas.

Figure 9a shows the transient effect of negative applied current on the rate of C₂H₄ oxidation for $P_{\text{C}_2\text{H}_4}/P_{\text{O}_2} \approx 0.55$. Under such conditions, and in general for $P_{\text{C}_2\text{H}_4}/P_{\text{O}_2}$ values less than approximately one, the rate decreases (electrophobic behavior). The rate decrease is modest (24%) in comparison with the open-circuit rate but is 200 times larger than $I/2F$ ($\Lambda = 200$).

The transient effect of negative current application under reducing conditions ($P_{\text{C}_2\text{H}_4}/P_{\text{O}_2} = 5$) is shown in Fig. 9b. In this case the catalytic rate increases ($\Lambda = -260$) and thus the reaction exhibits electrophilic behavior.

Steady-State Effect of Current

The above trends can be seen clearly in Figs. 10a and 10b which show the steady-state effect of current for oxidizing and reducing conditions, respectively. It can be seen that in the former case the rate of C₂H₄ oxidation increases

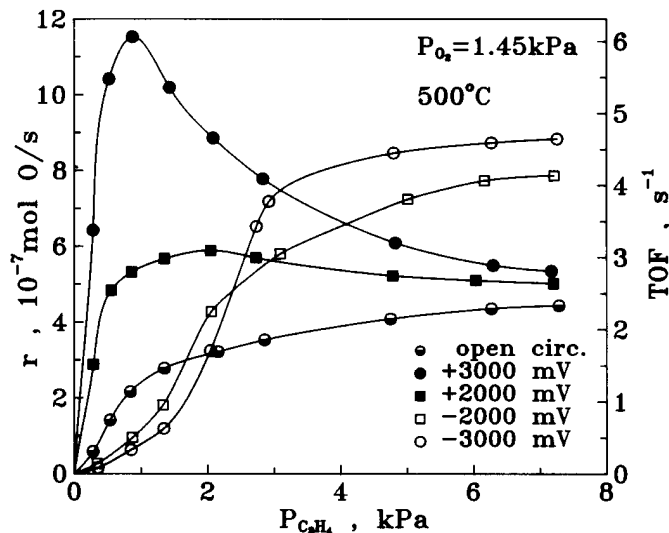


FIG. 11. Effect of $P_{C_2H_4}$ on the rate of C_2H_4 oxidation at various catalyst potentials.

monotonically with current ($\Lambda > 0$, electrophobic behavior), whereas under reducing conditions (Fig. 10b) the reaction exhibits electrophobic behavior for positive currents and electrophilic behavior for negative currents. Consequently, an “inverted volcano” plot (20, 21) is obtained. Measured Λ values are between -2000 and 2000 .

Effect of Gaseous Composition and Catalyst Potential

Figure 11 shows the effect of $P_{C_2H_4}$ and imposed catalyst potential at fixed P_{O_2} . The open-circuit (OC) behavior is also shown for comparison. Under OC conditions the rate exhibits a Langmuir-type behavior with respect to C_2H_4 , in agreement with previous studies of the same reaction on Pt/YSZ (2, 7). Positive potential application ($I > 0$) causes the appearance of a rate maximum which indicates enhanced binding and increased coverage of C_2H_4 on the surface. The rate maximum shifts to lower $P_{C_2H_4}$ values with increasing potential.

Negative applied potentials cause a decrease in the rate for low $P_{C_2H_4}$ values and an increase at high $P_{C_2H_4}$ values. The rate maximum disappears and “s-shaped” type behavior is obtained instead (Fig. 11).

The effect of P_{O_2} and catalyst potential at fixed $P_{C_2H_4}$ is shown in Fig. 12. Here a rate maximum vs P_{O_2} appears for negative applied potential. The rate is enhanced with increasing V_{WR} for high P_{O_2} values while the opposite trend is observed for low P_{O_2} values in accordance with the results of Fig. 11.

Figures 13a and 13b (which correspond to the conditions of Figs. 10a and 10b) demonstrate clearly the effect of catalyst potential V_{WR} , which is similar to that of current and also similar to that obtained in NEMCA studies of C_2H_4 oxidation utilizing YSZ (1, 2, 7) and $\beta''\text{-Al}_2O_3$ (6, 7). Under oxidizing conditions the rate increases monotonically with

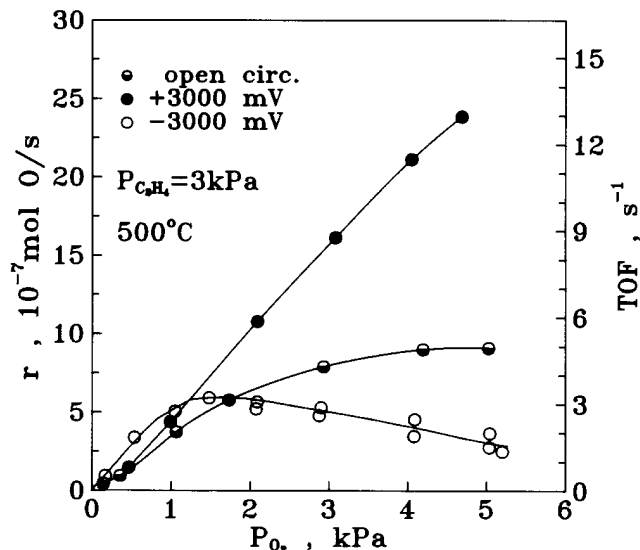


FIG. 12. Effect of P_{O_2} on the rate of C_2H_4 oxidation at various catalyst potentials.

V_{WR} (Fig. 13a, electrophobic behavior). Under reducing conditions inverted volcano behavior is observed (Fig. 13b). In the former case the rate varies typically by a factor of 10, in the latter only by a factor 2.

Compensation Effect

Figure 14a shows Arrhenius plots obtained at fixed values of catalyst potential V_{WR} for a fixed low (0.55) value of $P_{O_2}/P_{C_2H_4}$. Interestingly, increasing V_{WR} increases not only the catalytic rate but also the apparent activation energy E_a from 0.3 eV ($V_{WR} = -2$ V) to 0.9 eV ($V_{WR} = +2$ V) (Fig. 14b). This is due to a concomitant linear increase in the logarithm of the apparent preexponential factor TOF° of the turnover frequency TOF defined from

$$TOF = TOF^\circ \cdot \exp(-E_a/k_bT) \quad [5]$$

as in previous NEMCA studies (2, 7, 14). The linear variation in E_a and $\log(TOF^\circ)$ with V_{WR} (Fig. 14b) leads to the appearance of the well-known compensation effect (40, 42, 14). In the present case the isokinetic point ($T_\Theta = 300^\circ\text{C}$) lies outside the temperature range of the investigation.

Work Function Measurements

Figure 15a shows the effect of applied positive current on the potential V_{WR} and work function $e\Phi$ of the Pt catalyst film when it is exposed to oxidizing ($P_{O_2} = 5.4 \times 10^{-4}$ Pa) and reducing ($P_{H_2} = 3 \times 10^{-4}$ Pa) conditions in the high-vacuum chamber. The corresponding effect of negative current in oxidizing conditions ($P_{O_2} = 5.4 \times 10^{-4}$ Pa) is shown in Fig. 15b. In all cases the work function measurements were carried out after several (2–4) hours of exposure to the respective gaseous atmosphere.

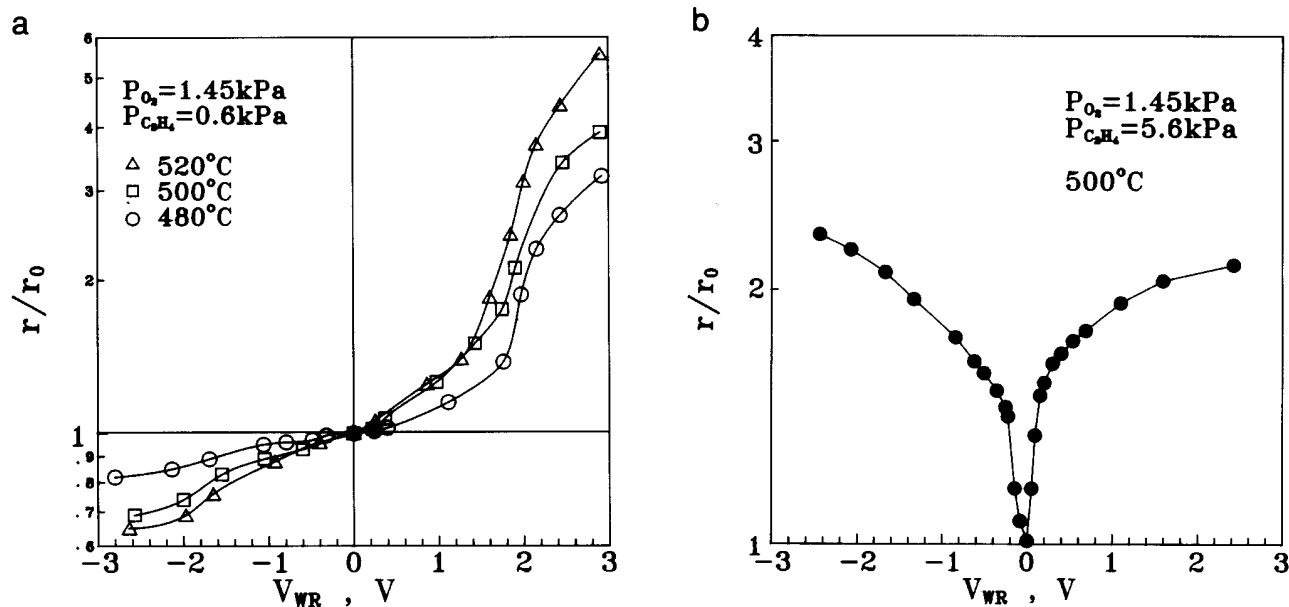


FIG. 13. Effect of catalyst potential on the rate of C₂H₄ oxidation on Pt/TiO₂ for high (a) and low (b) oxygen to ethylene ratios.

Under reducing conditions, current or potential application has no effect on the catalyst work function $e\Phi$ (Fig. 15a). This is consistent with the electronic (ohmic) nature of the current crossing the Pt–TiO₂ interface under these conditions.

Under oxidizing conditions, however, positive current application (Fig. 15a) leads to a substantial increase in

work function $e\Phi$ ($\Delta e\Phi = 1.4 \text{ eV}$) and negative current application (Fig. 15b) causes a substantial decrease in $e\Phi$ ($\Delta e\Phi = -0.4 \text{ eV}$). This behavior is similar to that observed when using solid electrolytes (such as YSZ or $\beta''\text{-Al}_2\text{O}_3$), in which case, as shown both theoretically (7) and experimentally (3, 39),

$$\Delta(e\Phi) = e\Delta V_{WR}. \quad [6]$$

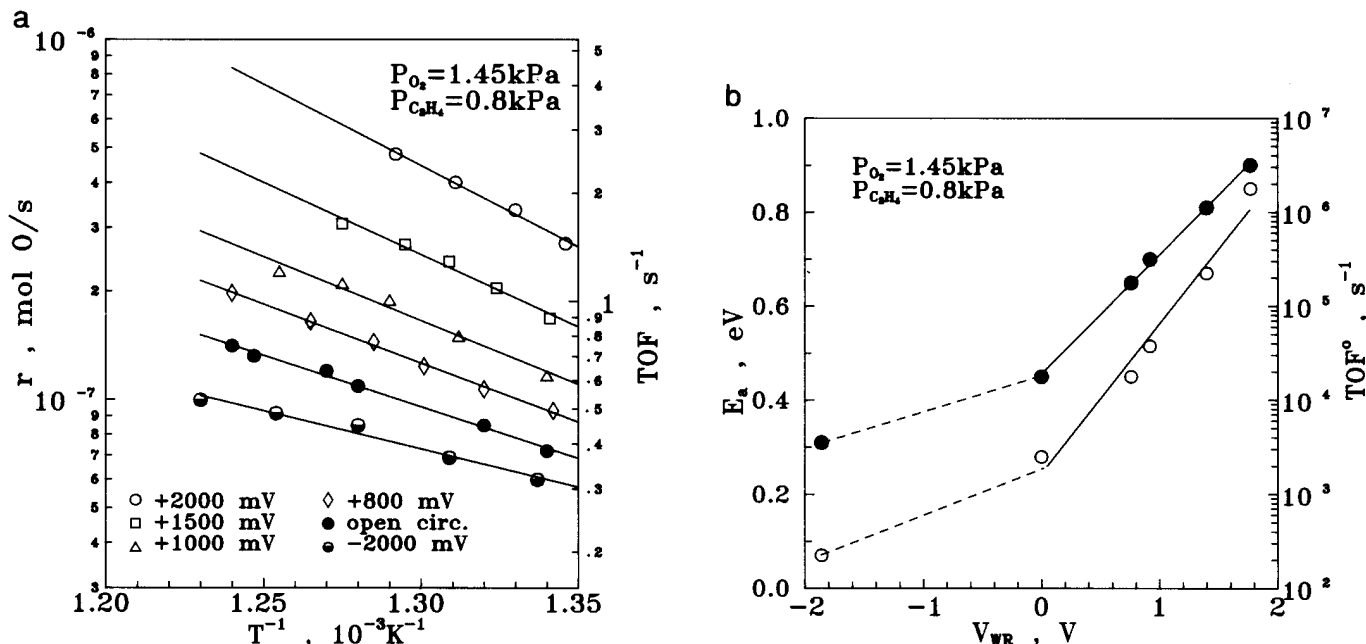


FIG. 14. (a) Arrhenius plots at various catalyst potentials. (b) Effect of catalyst potential on the apparent activation energy and preexponential factor of C₂H₄ oxidation on Pt/TiO₂.

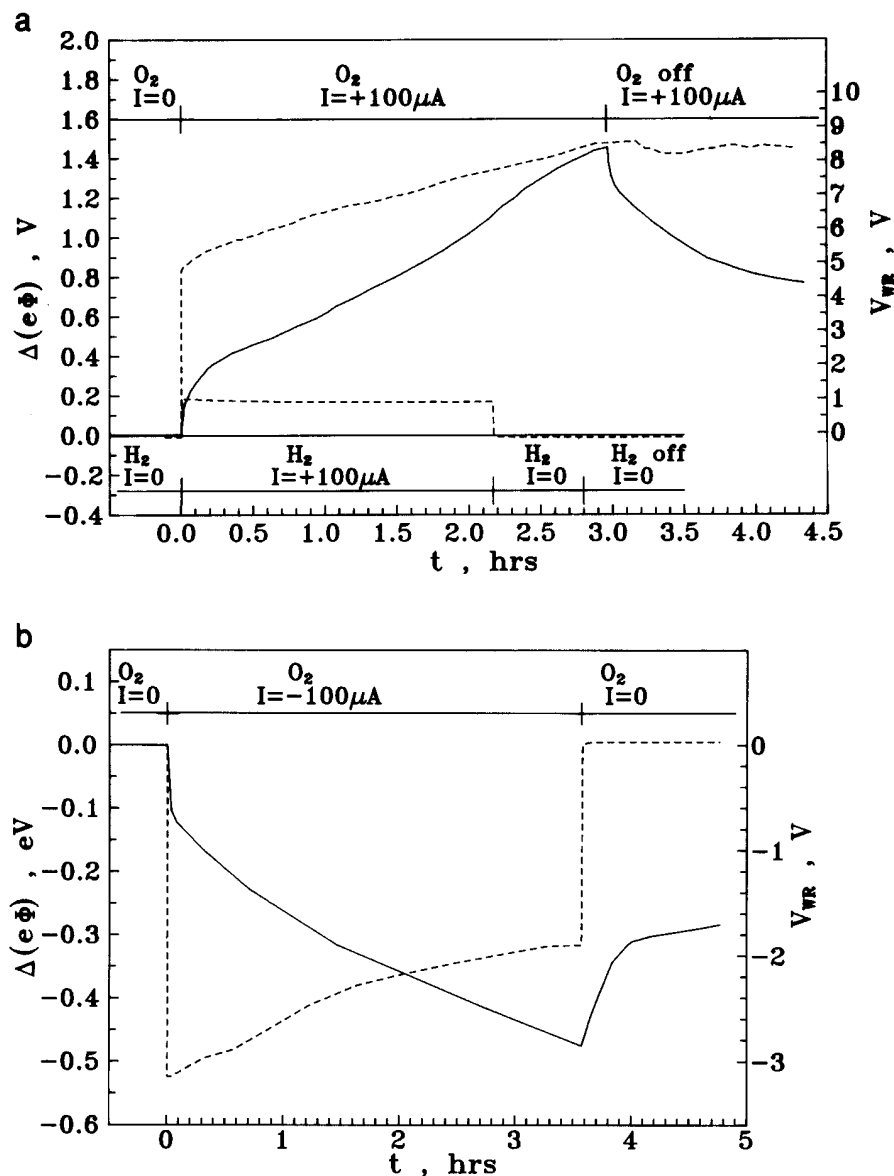


FIG. 15. (a) Transient effect of applied positive current on the catalyst potential (dashed line) and on the induced change in the catalyst work function (continuous line) under oxidizing and reducing conditions. In the latter case the work function remains constant; $P_{O_2} = 54$ mPa, $P_{H_2} = 30$ mPa, $T = 500^\circ\text{C}$. (b) Transient effect of applied negative current on the catalyst potential (dashed line) and on the induced change in the catalyst work function (solid line) under oxidizing conditions, $P_{O_2} = 54$ mPa, $T = 500^\circ\text{C}$.

In the present case of TiO_2 , which under oxidizing conditions is a mixed ionic–electronic conductor, one has

$$\Delta(e\Phi) = f e \Delta V_{\text{WR}}, \quad [7]$$

where $f \approx 0.15\text{--}0.2$ (Figs. 15a and 15b). The fact that the work function $e\Phi$ changes substantially with varying V_{WR} provides conclusive evidence that under oxidizing (and also atmospheric pressure reaction) conditions:

I. An electrochemical double layer is established at the Pt– TiO_2 interface (20).

II. Backspillover or spillover of ions is taking place

between the TiO_2 mixed conductor and the Pt catalyst surface.

These conclusions are further corroborated by the XPS measurements as shown below.

XPS Measurements

Figure 16 shows an XPS survey spectrum of the Pt/ TiO_2 catalyst electrode which shows no traces of impurities (e.g., C) on the Pt surface. The Ti $2p_{3/2}$ and O $1s$ peaks, with binding energies 458.3 and 529.4 eV, respectively, originate from the TiO_2 surface which is visible through microcracks of the

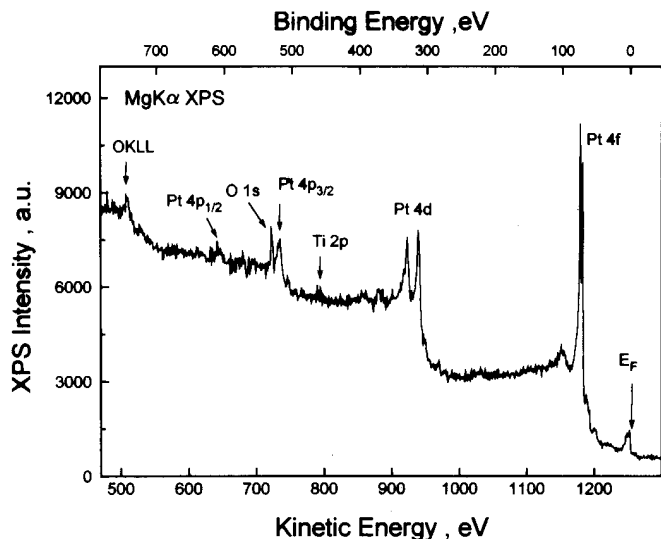


FIG. 16. XPS survey spectrum of the Pt/TiO₂ catalyst.

Pt catalyst film and not from TiO_x species on the film surface. This was confirmed by ion sputtering (Ar⁺ at 2 keV for 30 min) of the Pt film, which showed no measurable decrease in the Ti 2*p* and O 1*s* signals. The microcracks account for roughly 12% of the superficial surface area of the Pt film, as estimated from the relative intensities and sensitivities of the Ti 2*p*_{3/2} and Pt 4*f*_{7/2} peaks. This is in qualitative agreement with the SEM pictures (Fig. 3a).

Figure 17 shows the effect of prolonged oxygen exposure ($P_{O_2} = 5 \times 10^{-4}$ Pa for 3 h) on the O 1*s*, Ti 2*p*, and Pt 4*f* spectra. The Pt catalyst is grounded and thus species adsorbed on it can exhibit only chemical but not electrochemical shifts (16). The spectra of Fig. 17 were taken 15 min after pumping off oxygen or hydrogen. The high binding energy tail of the O 1*s* peak (Fig. 17a) is due to the presence of a higher O 1*s* binding energy state (~ 531 eV), which is attributed to hydroxyl species on the titania. A similar state was observed on Y₂O₃-doped ZrO₂ (16).

Oxygen exposure causes a shift (decrease) of 0.8 eV in the binding energies of O 1*s* and Ti 2*p* (Figs. 17a and 17b) without affecting the Pt 4*f* spectrum (Fig. 17c). This shift is reversible and disappears after exposure to H₂ ($P_{H_2} = 3 \times 10^{-3}$ Pa for 2 h).

The appearance of this shift verifies the development of an electrochemical double layer (20, 43, 44) at the Pt–TiO₂ interface under oxidizing conditions (Fig. 18), as also evidenced by the *I*-*V* and work function $e\phi$ measurements.

That is, under oxidizing conditions TiO₂ behaves, partly, as a solid electrolyte, due primarily to O²⁻ and to some extent H⁺ conduction, and consequently there is a charge separation and thus establishment of an electrochemical double layer, at the Pt–TiO₂ interface (Fig. 18), similar to the classical double layer existing at any metal–solid electrolyte (20) or metal–aqueous electrolyte (15, 43, 44) interface.

When such a double layer is established, the Fermi levels, (or electrochemical potentials of electrons (20) in the metal and in the electrolyte (μ_{Pt} and μ_{TiO_2} , respectively) deviate from each other (Fig. 18) and this deviation shows up as a shift in the Ti 2*p* and O 1*s*, XPS signals (Figs. 17a and 17b). Since the Pt electrode is grounded and thus fixed to the spectrometer Fermi level, only the Ti 2*p* and O 1*s* signals, originating from TiO₂, can shift.

One might expect this shift to be restricted to only those Ti and O atoms in the vicinity of the double layer (Fig. 18). These atoms are invisible to XPS due to the very large thickness (~ 10 μ m) of the porous Pt overlayer. However due to the significant conductivity and constancy of Fermi level in TiO₂ under these conditions, the XPS signals from all Ti and O atoms of the TiO₂ sample shift by the same amount in a manner similar to the case of the XPS investigation of the Pt/YSZ system (16). It is worth noting that, in the absence of any chemical shifts, the measured binding energy shift of Ti and O provides a direct measure of the difference in the Fermi levels or electrochemical potentials of electrons (7, 20) across the Pt–TiO₂ interface (0.8 V), i.e., TiO₂ becomes negative by 0.8 V with respect of Pt. The direct measurement of absolute potential differences across metal–electrolyte interfaces is one of the most challenging and yet unresolved problems in electrochemistry (43, 44). Changes in such potential differences can be easily measured via voltmeters (43, 44) or as electrochemical XPS shifts (16).

In the present case, however, the reversible creation and destruction of an electrochemical double layer at the Pt–TiO₂ interface provides the opportunity to measure directly, and probably for the first time, the absolute electrochemical potential difference across an electrochemical double layer.

The results of Fig. 17 are also in the same direction as expected from a Schottky barrier increase at the interface (33, 34) but the symmetric *I*-*V* behavior and the work function measurements are inconsistent with Schottky barrier model and consistent with the onset of a finite electrode–electrolyte charge transfer resistance. Furthermore in the case of a Schottky model one would expect no shift in the Ti and O core level binding energies of the exposed TiO₂ unless the characteristic length of the depletion (band bending) zone were comparable with the dimensions of the cracks (a few μ m). Consequently Fig. 17 most likely manifests the reversible creation (oxidizing conditions) and destruction (reducing conditions) of an electrochemical double layer at the Pt–TiO₂ interface.

Detailed examination of XPS spectra, such as the ones depicted in Fig. 17, under positive and negative current application, showed that positive currents increase the area under the O 1*s* spectrum by as much as 30% without causing any measurable change in the intensity of Ti 2*p* signal. Consequently there is no evidence for any significant electrochemically induced migration (backspillover)

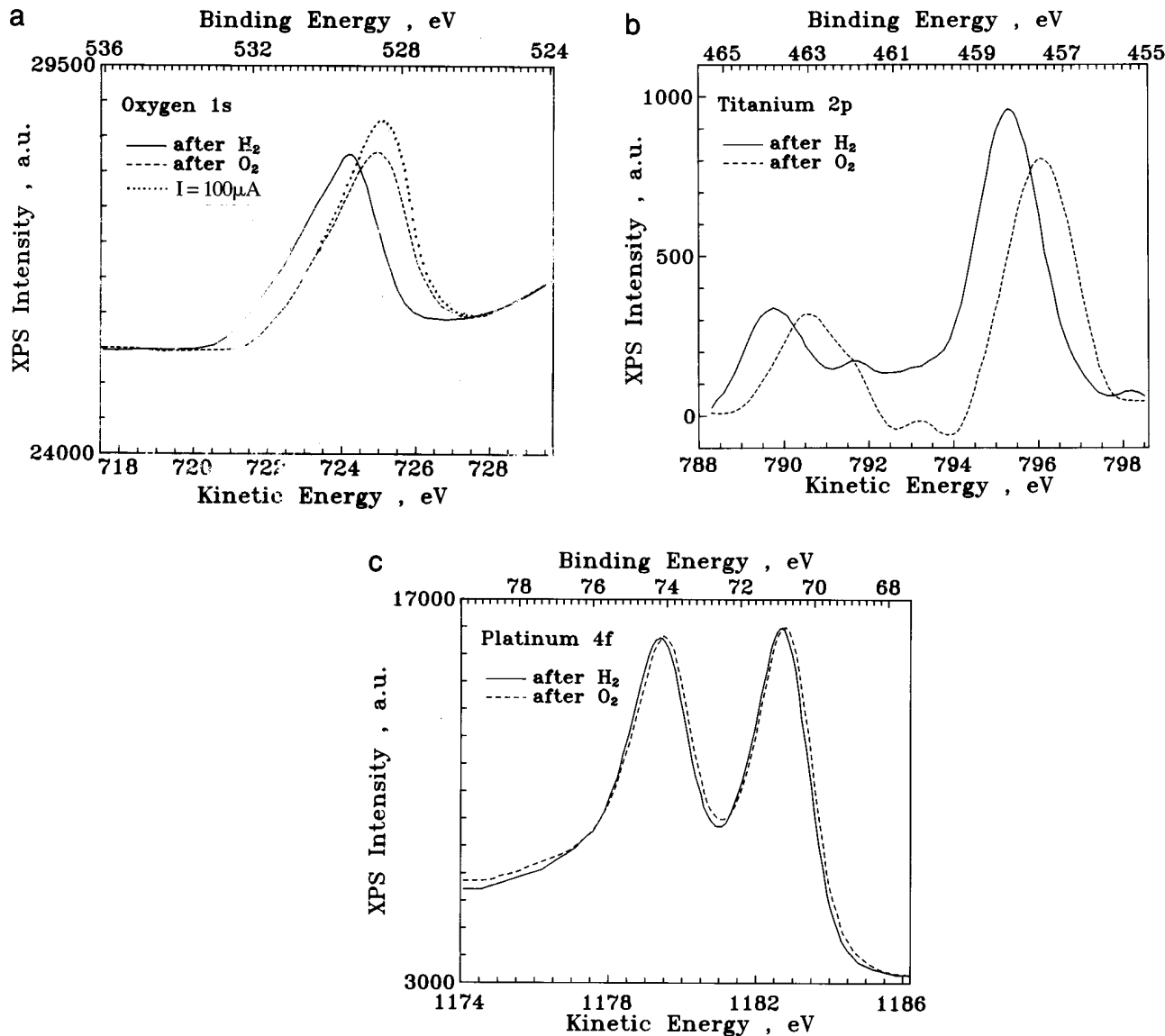


FIG. 17. Effect of O₂ and H₂ exposure on the XPS spectra of O 1s (a), Ti 2p (b) and Pt 4f (c); $P_{\text{H}_2} = 30$ mPa; $P_{\text{O}_2} = 54$ mPa, $T = 500^\circ\text{C}$, $I = 0$. Part a also shows the effect of positive current application ($I = 100 \mu\text{A}$ for 15 min under $P_{\text{O}_2} = 54$ mPa) on the O 1s XPS spectrum (dotted line). The current application had no detectable effect on the intensity of the Ti 2p and Pt 4f signals.

of TiO_x moieties on the Pt film surface. An example is shown in Fig. 17a. The increase in the O 1s, signal with positive currents (Fig. 17a) is similar to that observed with Pt films deposited on Y₂O₃-doped zirconia O²⁻-conducting solid electrolytes (16) and is consistent with the migration (backspillover) of ionically bonded oxygen on the Pt surface under positive bias in oxidizing environments. Note that the O 1s signal is due both to oxygen adsorbed on Pt and oxygen in the TiO₂ lattice, consequently the percentage increase in oxygen coverage on Pt under positive bias is significantly higher than the percentage area increase of the O 1s signal (16).

DISCUSSION

The present results establish, for the first time, that the effect of non-faradaic electrochemical modification of catalytic activity (NEMCA) (1–9, 12–21) or *in situ* controlled promotion (10) can be induced not only by solid electrolytes (1–14) but also by mixed conductors such as TiO₂, which is a mixed electronic–ionic conductor with predominantly electronic (*n*-type) conductivity.

The current–potential (Figs. 4–6), work function (Fig. 15) and XPS (Fig. 17) measurements are consistent with the idea that under reducing conditions in UHV the *n*-type

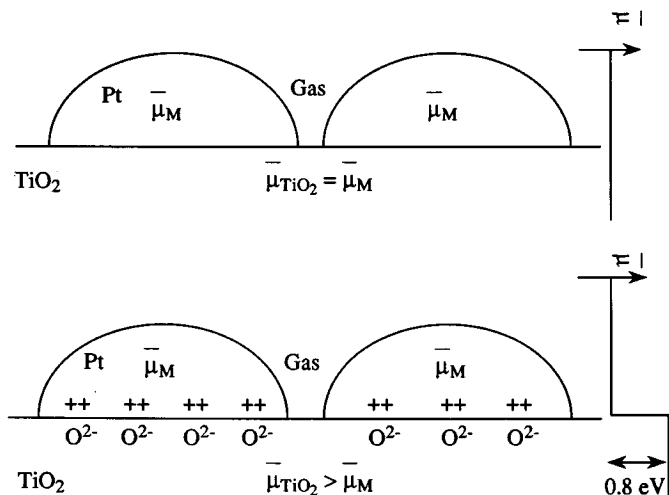


FIG. 18. Schematic diagram of the porous (and continuous) Pt film deposited on the TiO₂ sample under reducing conditions (top, electronic conduction in TiO₂, Ohmic Pt–TiO₂ contact) and under oxidizing conditions (bottom, mixed ionic–electronic conduction in TiO₂, presence of electrochemical double layer at the Pt–TiO₂ interface).

conductivity of TiO₂ totally dominates (Fig. 1) and consequently the Pt–TiO₂ contact is totally ohmic. Under these conditions there is no electrochemistry involved and no possibility to induce NEMCA by causing migration (backspillover) of promoting species from TiO₂ onto the Pt catalyst surface. This is also firmly established by the work function measurements in reducing environments (Fig. 15).

Under oxidizing conditions, however, and also under atmospheric pressure reaction conditions, the situation changes dramatically. The I - V_{WR} lines deviate from linearity (Figs. 4–6), the O 1s and Ti 2p binding energies shift by 0.8 eV in relation to Pt (Fig. 17) and, equally importantly, the work function of the Pt catalyst surface changes substantially by changing its potential (Fig. 15). The XPS shift of O 1s and Ti 2p manifests the creation of an electrochemical double-layer at the Pt–TiO₂ interface while the reversible work function changes show conclusively the electrochemically induced and controlled migration (backspillover) of species from TiO₂ onto the Pt surface.

This is accompanied by dramatic non-Faradaic enhancement in the catalytic rate of C₂H₄ oxidation, which demonstrates the promoting action of these backspillover species.

The XPS data, and in particular the observed enhancement in the O 1s signal with positive currents, in conjunction with the concomitant increase in work function $e\Phi$, shows that the migrating species is oxidic oxygen O^{δ-}, as in the case of Y₂O₃-stabilized ZrO₂ (YSZ) solid electrolytes (16).

In the case of negative currents, which also induce NEMCA (Figs. 9 and 10), the electrochemically migrating promoting species might be protons (37) in view of the recent ionic and protonic transport number measurements

of Norby and co-workers using the same TiO₂ samples as in the present work (38). A more general explanation, also operative in the case of NEMCA with YSZ (14, 20), is the following: In the presence of some finite ionic (O²⁻) conduction in TiO₂ accounting for a fraction f of the total conductivity, decrease ΔV_{WR} in catalyst potential has to cause a concomitant decrease $\Delta(e\Phi) = fe\Delta V_{WR}$ in the work function $e\Phi$ of the catalyst surface. In absence of migrating backspillover species (e.g., O²⁻, which can be supplied to the surface only with positive currents) the change in work function $\Delta(e\Phi)$ is necessarily associated with a change in the coverages θ_i and dipole moments P_i (C/m) of adsorbed species, which always have to satisfy the Helmholtz equation

$$\Delta(e\Phi) = -\frac{eN}{\epsilon_0} \sum \Delta(P_i\theta_i), \quad [8]$$

where $e = 1.6 \times 10^{-19}$ C/atom and N is the surface concentration of Pt atoms ($\sim 10^{19}$ atom/m²). Thus a negative $\Delta(e\Phi)$ can be accommodated by a decrease in the coverage of chemisorbed oxygen or a decrease in its dipole moment (7, 14), with a concomitant strengthening in the Pt=O chemisorptive bond since oxygen is an electron acceptor (7). When the solid electrolyte has a finite proton conductivity, as is the case here (38), then this decrease in oxygen coverage with negative currents may result from direct reaction with protons.

Regarding the fraction f of ionic conductivity of TiO₂ in oxidizing conditions it is worth noting the good qualitative agreement of the values estimated (~ 0.15) from the work function measurements (Fig. 15) and of those estimated from the relaxation time constants τ during galvanostatic transients (Figs. 8 and 9) in conjunction with $\tau \approx 2FN/fI$. The latter observation further corroborates that electrochemically controlled migration of O²⁻ onto the catalyst surface is the cause of the observed pronounced non-Faradaic rate enhancements (Figs. 8 to 14).

After establishing that NEMCA induced with TiO₂ has the same physicochemical origin with NEMCA induced with YSZ, i.e., electrochemically controlled oxide ion migration, or with β'' -Al₂O₃ i.e., electrochemically controlled migration of sodium, one can use the simple rule regarding promotion used to rationalize all previous NEMCA studies (1–15). It thus becomes possible to explain all the observed effects of catalyst potential V_{WR} and work function $e\Phi$ on the rate of C₂H₄ oxidation, including the observed dependence of the activation energy E_a on V_{WR} and the appearance of the compensation effect.

The rule is that increasing catalyst potential V_{WR} and work function $e\Phi$ causes a weakening in the binding strength of electron acceptor adsorbates, such as dissociatively chemisorbed oxygen and a strengthening in the chemisorptive bond strength of electron donor adsorbates, such as adsorbed ethylene. Conversely, decreasing V_{WR} and $e\Phi$ cause an increase in the binding strength of electron

acceptor adsorbates and a decrease in the binding strength of electron donor adsorbates.

We thus first refer to Figs. 10a and 13a, which depict the effect of current and potential, respectively, on the rate of C_2H_4 oxidation under oxidizing conditions. As can be seen from Fig. 11 the rate is and remains positive order in C_2H_4 under these conditions. As can also be inferred from Fig. 12, the open-circuit rate is practically zero-order in oxygen. These observations imply that the Pt surface is predominantly covered with oxygen and with very little adsorbed ethylene. Increasing V_{WR} enhances the binding of ethylene on the catalyst surface and weakens the Pt=O bond. Both factors enhance the catalytic rate, as at the limit of very high V_{WR} , the ratio of the surface coverages θ_O and $\theta_{C_2H_4}$ of oxygen and ethylene, respectively, approaches unity, which tends to maximize the rate. This is manifested both in Fig. 11, where for $V_{WR} = 2$ and $3V$ the rate exhibits a maximum with $P_{C_2H_4}$, even at $P_{C_2H_4} = 0.4$ kPa, and in Figs. 10a and 13a, where the rate approaches a plateau with increasing current and V_{WR} , respectively.

The weakening in the binding of chemisorbed oxygen with increasing V_{WR} is also manifested in Fig. 12, which shows that for high P_{O_2} the rate shifts from zero-order in oxygen under open-circuit conditions to near first-order with $V_{WR} = 3V$.

We then refer to Figs. 10b and 13b, which show the effect of current and potential, respectively, under net reducing gas-phase compositions. As can be noted from Figs. 11 and 12, under this gaseous composition the open-circuit rate is already approaching a plateau for both ethylene and oxygen, implying high and nearly equal coverages on the catalyst surface. Consequently the potential-induced rate enhancement is only moderate ($\rho = r/r_O < 2.3$) both for positive and for negative overpotentials. The rate enhancement with positive currents and overpotentials can be rationalized, as previously, on the basis of the weakening of the Pt=O bond. The approach to a plateau with increasing V_{WR} can be attributed to the concomitant decrease in oxygen coverage as manifested by the approach to linearity in the rate vs P_{O_2} behavior (Fig. 12).

The rate enhancement with negative currents and overpotentials can be rationalized on the basis of concomitant weakening of the Pt- C_2H_4 bond. This is also manifested in Fig. 11. Negative potentials, which weaken the binding and decrease the coverage of ethylene, suppress the rate for low $P_{C_2H_4}$ values, as they further decrease the already low coverage of ethylene but enhance the rate for high $P_{C_2H_4}$, where the ethylene coverage is excessively high.

On the basis of the above, Figs. 11 and 12 can be rationalized immediately. Increasing V_{WR} enhances the binding of C_2H_4 on Pt and this causes the gradual transition from an "s-shaped" rate dependence to the development of a rate maximum, which shifts to lower $P_{C_2H_4}$ with increasing V_{WR} (Fig. 11). Increasing V_{WR} weakens the binding of oxygen

on the Pt surface and this causes the disappearance of the rate maximum ($V_{WR} = -3V$) and the development of linear kinetics for $V_{WR} = 3V$ (Fig. 12).

The observed increase in the apparent activation energy with V_{WR} is at first surprising in view of the fact that NEMCA studies of C_2H_4 oxidation of Pt/YSZ (2, 7) have shown a pronounced activation energy decrease (from 1.1 to 0.4 eV) with increasing V_{WR} at temperatures below 380°C.

That study (2, 7), performed at significantly lower temperatures than the present one, provided no evidence of strong ethylene adsorption for V_{WR} values up to 1V. In the present case the observed increase in E_a with V_{WR} must be attributed to the strengthening of the Pt- C_2H_4 bond with increasing V_{WR} , which overbalances the concomitant decrease in the binding strength of oxygen.

As shown in Fig. 14, the observed pronounced rate enhancement is due to the dramatic increase in the apparent preexponential factor with increasing V_{WR} . Since the apparent preexponential factor contains the product, $\theta_O \cdot \theta_{C_2H_4}$, of the surface coverages of oxygen and ethylene, it follows that the observed dramatic increase is primarily due to the increase in $\theta_O \cdot \theta_{C_2H_4}$ with increasing V_{WR} due to the pronounced enhancement in the binding of ethylene. The NEMCA-induced compensation effect has been discussed elsewhere (14, 20, 21).

CONCLUSIONS

Titania can be used as an active catalyst support to reversibly enhance the catalytic activity of Pt for C_2H_4 oxidation by up to a factor of 20 via potential application. The observed rate increase is up to 2000 times larger than $I/2F$. The observed phenomena appear to be very similar to previous NEMCA studies utilizing O^{2-} conductors, such as YSZ, and are due to electrochemically controlled migration of oxidic species onto the catalyst surface. These oxidic species act as promoters by modifying the work function of the surface and the binding strength of reactants and intermediates. Proton transport to the catalyst upon negative current application may also play a role. The use of XPS upon switching from reducing to oxidizing conditions in UHV allows for the study of the formation and destruction of an electrochemical double layer at the Pt-TiO₂ interface and for an approximate measurement the absolute potential difference (0.8 V) across that interface. Such measurements are not possible with Pt/YSZ interfaces since in that case the electrochemical double layer is always present (16, 20).

The use of mixed conductors, such as TiO₂, to induce NEMCA is of considerable theoretical and practical interest. The possible relationship of the present phenomena with SMSI is worth investigating.

ACKNOWLEDGMENTS

We thank the Stride-Hellas and CEC Science programs for financial support Mr. Th. Pallis for the SEM, and our reviewers for helpful comments.

REFERENCES

1. Vayenas, C. G., Bebelis, S., and Neophytides, S., *J. Phys. Chem.* **92**, 5083 (1988).
2. Bebelis, S., and Vayenas, C. G., *J. Catal.* **118**, 125 (1989).
3. Vayenas, C. G., Bebelis, S., and Ladas, S., *Nature* **343**, 625 (1990).
4. Pritchard, J., *Nature* **342**, 592 (1990).
5. Politova, T. I., Sobyenin, V. A., and Belyaev, V. D., *React. Kinet. Catal. Lett.* **41**, 321 (1990).
6. Vayenas, C. G., Bebelis, S., and Despotopoulou, M., *J. Catal.* **128**, 415 (1991).
7. Vayenas, C. G., Bebelis, S., Yentekakis, I. V., and Lintz, H. G., *Catal. Today* **11**, 303 (1992).
8. Cavalca, C. A., Larsen, G., Vayenas, C. G., and Haller, G. L., *J. Phys. Chem.* **97**, 6115 (1993).
9. Marina, O. A., and Sobyenin, V. A., Belyaev, V. D., and Parmon, V. N., *Catal. Lett.* **13**, 567 (1992).
10. Yentekakis, I. V., Moggridge, G., Vayenas, C. G., and Lambert, R. M., *J. Catal.* **146**, 292 (1994).
11. Harkness, I. R., and Lambert, R. M., *J. Catal.* **152**, 211 (1995).
12. Cavalca, C. A., and Haller, G. L., submitted.
13. Varkaraki, E., Nicole, J., Plattner, E., Comninellis, Ch., and Vayenas, C. G., *J. Appl. Electrochem.* **25**, 978 (1995).
14. Pliangos, C., Yentekakis, I. V., Verykios, X. E., and Vayenas, C. G., *J. Catal.* **154**, 124 (1995).
15. Neophytides, S. G., Tsiplakides, D., Stonehart, P., Jaksic, M. M., and Vayenas, C. G., *Nature* **370**, 45 (1994).
16. Ladas, S., Kennou, S., Bebelis, S., and Vayenas, C. G., *J. Phys. Chem.* **97**, 8845 (1993).
17. Basini, L., Cavalca, C. A., and Haller, G. L., *J. Phys. Chem.* **98**, 10853 (1994).
18. Neophytides, S., and Vayenas, C. G., *J. Phys. Chem.* **99**, 17063 (1995).
19. Vayenas, C. G., Ladas, S., Bebelis, S., Yentekakis, I. V., Neophytides, S., Jiang, Yi, Karavasilis, Ch., and Pliangos, C., *Electrochimica Acta* **39**(11/12), 1849 (1994).
20. Vayenas, C. G., Jaksic, M. M., Bebelis, S. I., and Neophytides, S. G., in "Modern Aspects of Electrochemistry" (J. O'M., Bockris, B. E. Conway, and R. E. White, Eds.), Vol. 29, pp. 57–202. Plenum, New York, 1995.
21. Vayenas, C. G., and Yentekakis, I. V., in "Handbook of Heterogeneous catalysis" (G. Ertl, H. Knötzinger, and J. Weitkamp, Eds.), VCH, Weinheim, New York, in press.
22. Bockris, J. O' M., and Minevski, Z. S., *Electrochimica Acta* **39**(11/12), 1471 (1994).
23. Tauster, S. J., Fung, S. C., and Garten, R. L., *J. Am. Chem. Soc.* **100**, 170 (1978).
24. Resasco, D. E., and Haller, G. L., *J. Catal.* **82**, 279 (1983).
25. Cairns, J. A., Baglin, J. E., Clark, G. L., and Zeigler, J. F., *J. Catal.* **83**, 301 (1983).
26. Belton, D. N., Sun, Y. M., and White, J. M., *Phys. Chem.* **88**, 1690 (1984).
27. Ko, C. S., and Gorte, R. J., *J. Catal.* **90**, 59 (1984).
28. Tauster, S. J., *Acc. Chem. Res.* **20**, 389 (1987).
29. Haller, G. L. and Resasco, D. E., *Adv. Catal.* **36**, 173 (1987).
30. Göpel, W., *Sensors Actuators B* **18–19**, 1 (1994).
31. Balachaudran, U., and Eror, N. G., *J. Mater. Sci.* **23**, 2676 (1988).
32. Göpel, W., Kirner, U., and Wiemhöfer, H. D., *Solid State Ionics.* **28–30**, 1423 (1988).
33. Schierbaum, K. D., Kirner, U. K., Geiger, J. F., and Göpel, W., *Sensors Actuators B* **4**, 87 (1991).
34. Schierbaum, K. D., Wei-Xing, X., and Göpel, W., *Ber. Bunsenges. Phys. Chem.* **97**, 363 (1993).
35. Douglas, D. L., in "Selected Topics in High Temperature Chemistry" (O. Johannessen and A. G. Andersen, Eds.), pp. 192–194, Elsevier, NY 1989.
36. Gellings, P. J., and Bouwmeester, H. J. M., *Catal. Today* **12**, 1 (1992).
37. Norby, T., *Solid State Ionics* **40/41**, 857 (1990).
38. Thurmann-Nielsen, A., and Norby, T., in preparation.
39. Ladas, S., Bebelis, S., and Vayenas, C. G., *Surf. Sci.* **251–252**, 1062 (1992).
40. Schwab, G.-M., *Advan. Catal.* **2**, 251 (1950).
41. Cremer, E., *Advan. Catal.* **7**, 7 (1955).
42. Schwab, G.-M., *J. Catal.* **84**, 1 (1983).
43. Bockris, J. O' M., and Khan, S. U. M. in "Surface Electrochemistry" Plenum, New York, 1993.
44. Trasatti, S., *Pure Appl. Chem.* **58**(7), 955 (1986).